SUPPORTING INFORMATION:

Stability of protein-specific hydration shell on crowding

Kuo-Ying Huang[†], Carolyn N. Kingsley[§], Ryan Sheil[†], Chi-Yuan Cheng, Jan C. Bierma[‖], Kyle W. Roskamp[§], Domarin Khago[§], Rachel W. Martin*[,§,‖], Songi Han*[,†,‡]

[†]Department of Chemistry and Biochemistry, University of California, Santa Barbara, CA 93106

[‡]Department of Chemical Engineering, University of California, Santa Barbara, CA 93106

[§]Department of Chemistry, University of California, Irvine, CA 92697

[‖]Department of Molecular Biology and Biochemistry, University of California, Irvine, CA 92697

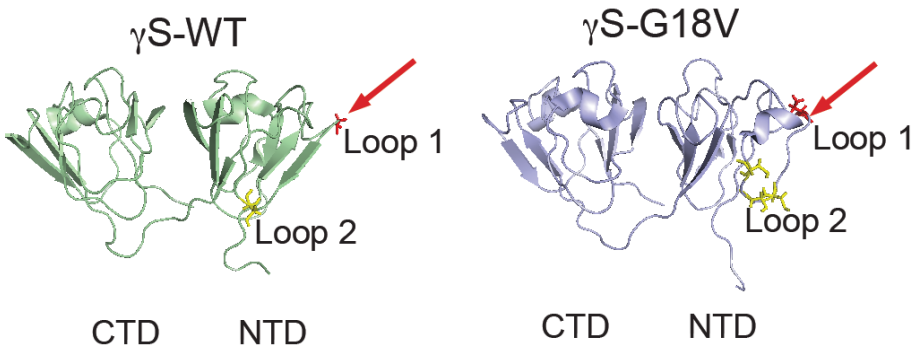

Figure S1: The solution NMR structures of wild-type (green) and G18V (blue) γS-crystallin under monomeric conditions are shown with pertinent residues highlighted. The labels NTD and CTD refer to the N-terminal domain and C-terminal domain, respectively. The G18V mutation site, located in Loop 1 of the NTD, is highlighted in red. The solvent-accessible cysteines located in Loop 2 are marked in yellow.

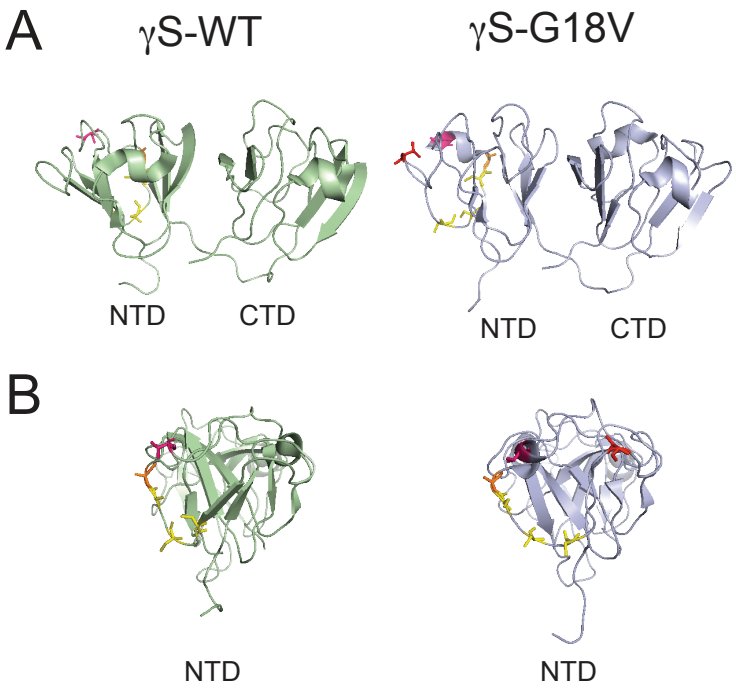

Figure S2: A. The solution NMR structures of wild-type (green) and G18V (blue) γS-crystallin. Residues 23, 25, and 27 (shown in yellow), indicate the cysteine residues located in Loop 2 of the N-terminal domain. B. Detail of the N-terminal domain, showing some of the relevant residues. The alanine at position 28, shown in orange, and the threonine at position 32, shown in pink, were mutated to cysteines in separate constructs in order to introduce new spin labeling sites.

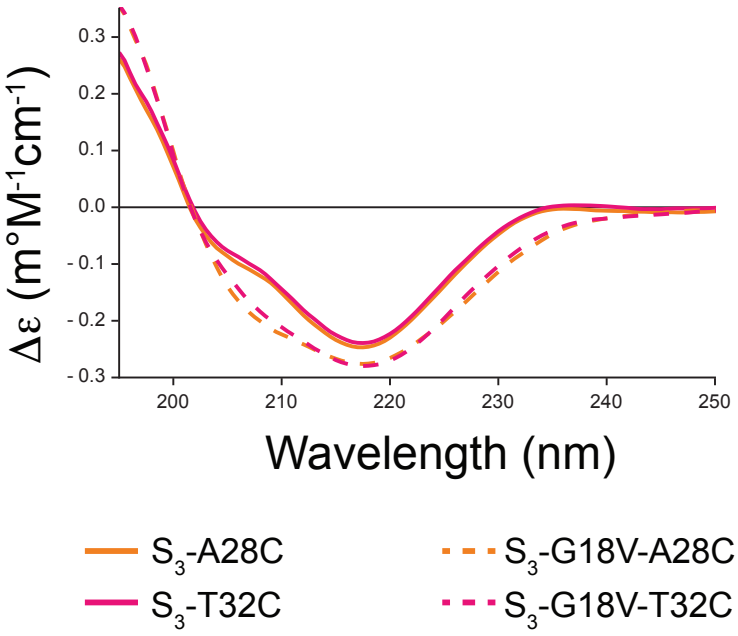

Figure S3: CD spectra of S_3-variants. Samples were concentrated to 0.10 mg/mL in 10 mM sodium phosphate (pH 6.9) with 0.05 % NaN_3. Spectra were measured in triplicate over the wavelength range from 260 nm to 195 nm. Measurement parameters were 50 nm/sec continuous scanning with a 2 nm bandwidth and 4 sec response. The CD spectra indicate mostly β-sheet secondary structure and are consistent with those previously measured for γS-WT and γS-G18V.[1]

1. A local conformational change around Loop 2 was found in γS-WT

Concentration-dependent changes in γS-WT conformation around the endogenous spin labeling site were assessed by CWEPR spectra. The wild-type protein stored initially at high concentration (>100 mg/ml) showed a characteristic broadened EPR linewidth indicating a less mobile spin probe regardless of the concentration at which the data was measured, while the protein initially stored at lower concentration (<100 mg/ml) showed a relatively sharper line width even when concentrated to 270 mg/ml (See Figure 1). The spectral line-shape showed a dependence upon the initial protein concentration prior to spin labeling—but remained relatively static over concentration changes post spin labeling—which is indicative of a protein conformational change or intermolecular interaction occurring at a specific concentration (>100 mg/ml), subsequently preserved (becomes irreversible) upon spin labeling. Furthermore, spin labeling the protein before the interaction occurs (<100 mg/ml) blocks this interaction from forming upon

concentrating. This led us to believe that the discrepancy in the EPR line-shape was due to the formation of a disulfide bond, as the MTSL (spin probe) binds to free cysteine residues.

A compound that cleaves disulfide bonds, DTT (5mM), was added to the high initial concentration sample, then washed from the sample prior to spin labeling. The EPR line-shape of the DTT-treated sample narrowed significantly, becoming very similar to the low initial concentration spectra. Figure S2 presents the EPR spectra of the high and low initial concentration samples (EPR spectra measured at the same concentration), showing the line-shape dependence on initial concentration and the effect of the DTT treatment. In contrast to an EPR line-shape of γS-WT, which is protein concentration-dependent prior to spin labeling, no protein concentration dependence was found in the γS-WT hydration dynamics. From this data along with previous measurements indicating that the wild type protein exists as monomer in solution even at high concentration, we hypothesize that the change in protein dynamics found in the CWEPR spectra, may be due to the formation of an *intramolecular* disulfide bond between two cysteines in the loop2 region (between C23 and C27). The formation of an intramolecular disulfide could restrict the protein backbone motion causing a change to be observed by EPR, without significantly changing the hydration landscape near the spin-label (shown in figure S2). The intramolecular disulfide bond between C23 and C27 could stabilize the protein by preventing the cysteine residues from forming intermolecular disulfide bonds at high concentration or upon aggregation of the protein.

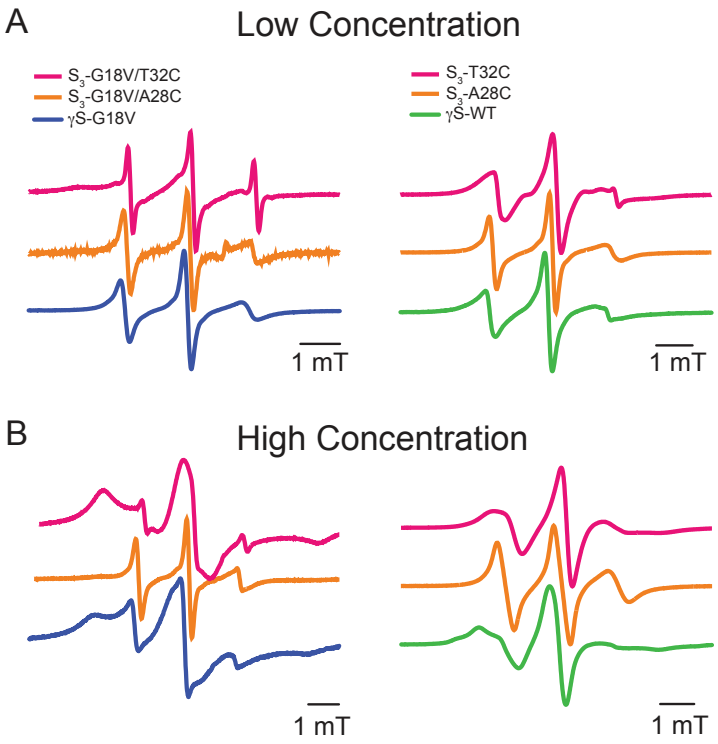

Figure S4: CWEPR spectra of γS-G18V (left) and γS-WT (right) with all variants at low and high concentrations.

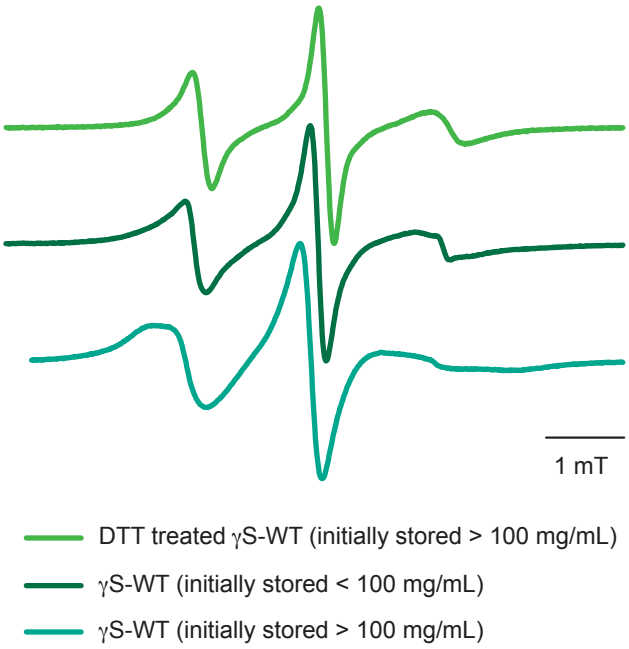

Figure S5: CWEPR spectra of γS-WT at different initial storing protein concentrations along with the DTT treated high protein concentration sample. The wild type EPR spectra showed a dependence on the initial storing condition that once spin-labeled was irreversible with dilution after spin labeling. Initial protein storing conditions: 5 mg/ml (black), 150 mg/ml (red), 5 mM DTT pre-treated at 150 mg/ml (blue), while all spectra were measured at low protein concentration (< 15 mg/ml) and

their intensities normalized.

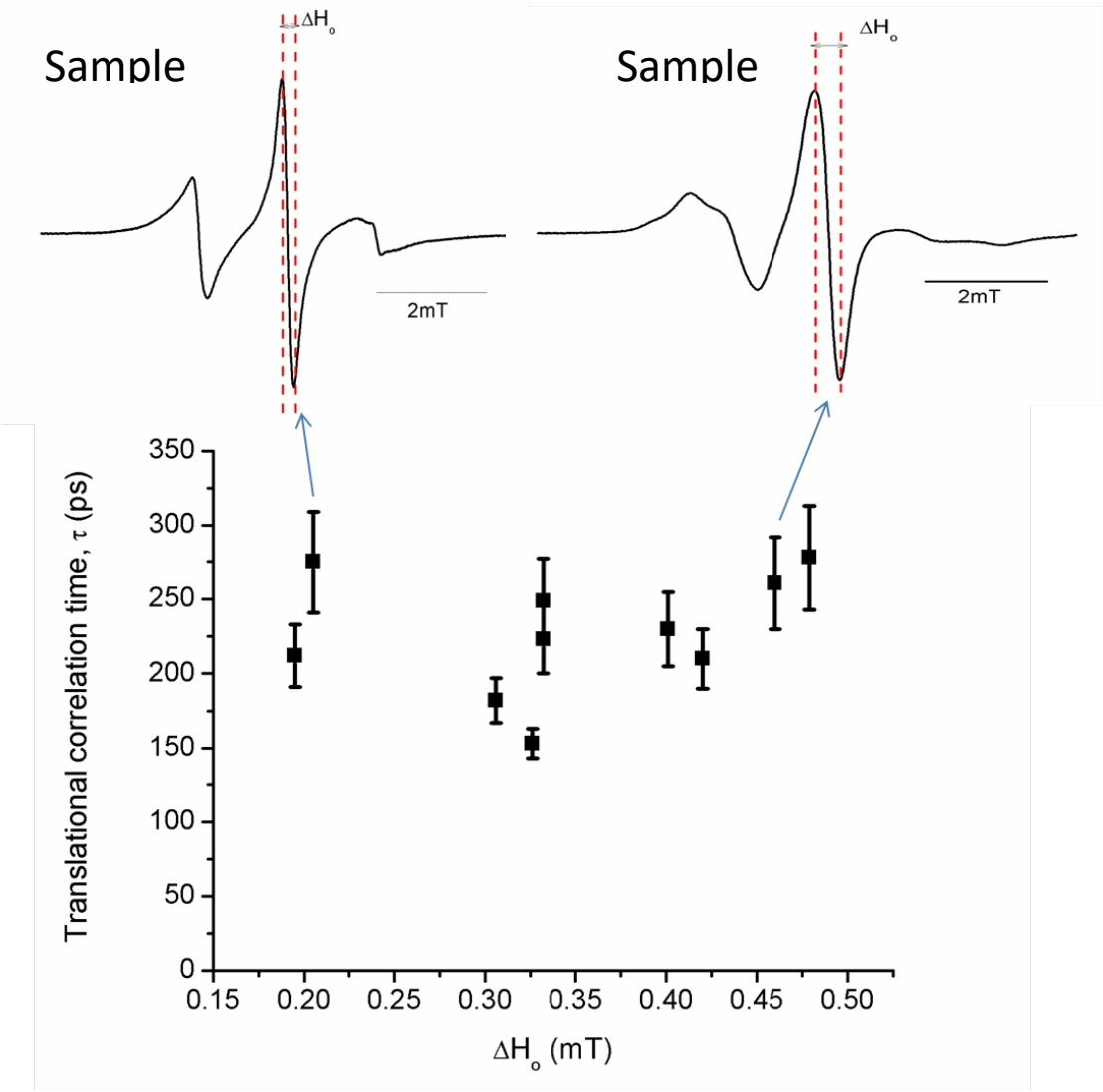

Figure S6: ODNP measured translational correlation time of γS-WT surface hydration and corresponding spin label mobility characterized by EPR line width of the central transition (ΔH_o). γS-WT hydration dynamics were not affected by the changes in the spin label mobility (conformational changes) seen in CWEPR.

2. Viscosity effect on γS-WT EPR line-shape at high concentrations

A broadening in EPR line-shape was observed above concentrations of 350 mg/ml in the γS-WT. In order to test if this was simply due to an increase in solution viscosity with increasing protein concentration, we added sucrose systematically to a sample of low protein concentration (15 mg/ml), shown in figure S4. In this way, we were able to see purely the effect of viscosity on the EPR line-shape. At ~55 weight percent

sucrose, the EPR line-shape resembled that of the high protein concentration sample (350 mg/ml). This indicates that at higher concentrations the broadening in line-shape is most likely due to an increase in solution viscosity with increasing protein concentration.

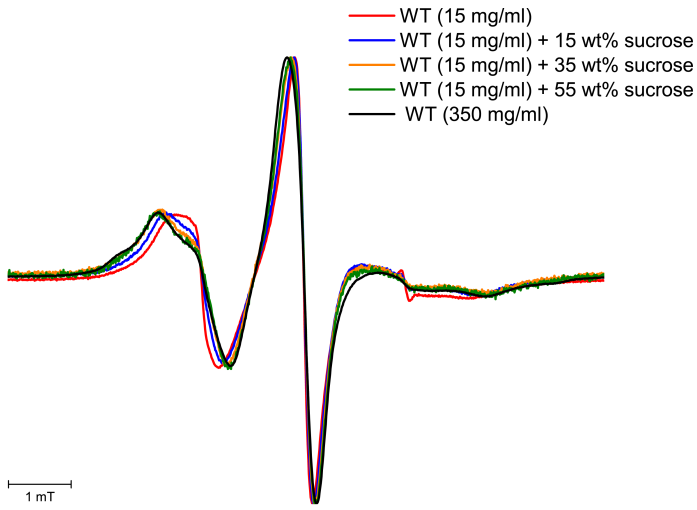

Figure S7: CWEPR spectra of the wild type protein with varying amounts of sucrose added to systematically change the viscosity. As sucrose was added to the low concentration sample, the EPR line-shape approached the broadened line-shape characteristic of more highly concentrated sample. At ~55 weight percent sucrose added to 15 mg/ml of γS-WT, the EPR spectra of the looked very similar to the spectra of the 350 mg/ml protein sample without the addition of sucrose.

3. ODNP Theory

Here, we only provide a brief summary of ODNP theory; a more detailed description can be found in the literature[2-4]. Solution state ODNP relies on the transference of the polarization of a saturated EPR transition—effectively enhancing the proton NMR signal of water within close proximity to a nitroxide spin-label.[4] The maximum NMR signal enhancement is given by eq. 1[5], where ξ, is the coupling constant, f, is the leakage factor, s_{max} is the maximum electron saturation factor, and $|\omega_E/\omega_H|$ is the gyromagnetic ratio of the electron and nuclear spins.

$$Lim_{p\to\infty}E(p) = E_{\max} = 1 - \xi s_{\max} f \left|\frac{\omega_e}{\omega_H}\right| \qquad \text{Eq. 1}$$

$$f = 1 - \frac{T_1}{T_{1,0}^{-1}} \qquad \text{Eq. 2}$$

The coupling constant, ξ, is the key parameter to extract hydration dynamics information from ONDP enhancement. However, equation 1 does not take the dielectric heating (sample heating due to microwave irradiation) into consideration. Therefore, the resultant coupling constant would be overestimated due to the dielectric heating. A new expression including a correction for dielectric heating is shown in eqs. 3, 4, and 5, where k_ρ is the cross relaxation rate and k_σ is the local self-relaxation rate [2].

$$\xi = \frac{k_\sigma}{k_\rho} \qquad \text{Eq. 3}$$

$$k_\sigma \approx k_\sigma s_{\max} = Lim_{p\to\infty}\left[\frac{1-E(p)}{(C)T_1(p)}\left|\frac{\omega_e}{\omega_H}\right|\right] \qquad \text{Eq. 4}$$

$$k_\rho = \frac{T_1(0)^{-1} - T_{1,0}(0)^{-1}}{C} \qquad \text{Eq. 5}$$

By measuring the proton longitudinal relaxation time $T_1(p)$ and the proton NMR signal enhancement as a function of microwave power, one can extrapolate to obtain $k_\sigma S_{max}$ in equation 4. For biological samples with tethered spin probes or free nitroxides in high concentration (~100mM), an approximation of $s_{max} = 1$ is reasonable. By measuring the T_1 time without the presence of microwave power of two samples one with and one without the presence of spin-label ($T_{1,0}$ (0)), k_ϱ can be calculated (eq. 5). Once k_σ and k_ϱ are both calculated, one is able to calculate the experimental value for the coupling constant, ξ.

The coupling constant is described by the spectral density function, $J(\omega)$, for the dipolar interaction between the electron (spin-probe) and the proton (water), where fluctuations in the dipolar interaction are dominated by translational diffusion. From this, we employ Hwang and Freed's expression[6], for the spectral density function, which is based on a force free hard sphere model (FFHS) (eq. 6).

$$J(\omega;\tau) = \Re e\left[\frac{1+\frac{z}{4}}{1+z+\frac{4z^2}{9}+\frac{z^3}{9}}\right] \qquad \text{Eq. 6}$$

$$z = \sqrt{i\omega\tau}$$

The coupling constant is described in eq. 7, where B_0 is the static field used in the experiment corresponding to NMR frequencies near $\omega_H/2\pi$ = 15 MHz.

$$\xi(B_0;\tau) = \frac{6J(\omega_e - \omega_H;\tau) - J(\omega_e + \omega_H;\tau)}{6J(\omega_e - \omega_H;\tau) + 3J(\omega_H;\tau) + 6J(\omega_e + \omega_H;\tau)}$$

$$\omega_e = \gamma_e B_0 \qquad \text{Eq. 7}$$

$$\omega_H = \gamma_H B_0$$

By determining the value of τ_c, that produces the experimentally measured coupling constant in eq. 7 we are able to extract the experimental correlation time, which corresponds to the time for water to diffuse within 5~15Å of the spin label. Larger values for the correlation time correspond to slower hydration dynamics while smaller values refer to faster hydration dynamics. A systematic approach has been developed for proteins, vesicles, and polymers to characterize correlation times that correspond to free, surface-exposed, intermediate, and buried spin-labels.

4. δΔ /ΔT data

2D ^{1}H-^{15}N HSQCs were collected for both γS-WT and γS-G18V every 5 °C as the samples were heated between 22-47 °C. These data were acquired on an 800 MHz Varian ^{Unity}INOVA spectrometer (Agilent, Inc.) equipped with a ^{1}H-^{13}C-^{15}N 5 mm tri-axis PFG triple resonance probe Decoupling of ^{15}N nuclei were performed using the GARP sequence.[7] The samples were allowed to equilibrate at each temperature for several minutes before data collection. Sample precipitation and loss of signal occurred at temperatures above 47 °C. ^{1}H shifts were referenced to TMSP and ^{15}N shifts were referenced indirectly to TMSP. NMR data were processed using NMRPipe and analyzed using Sparky. N-H δΔ /ΔT values were measurable for 134 of 178 residues in γS-WT and 138 / 178 residues in γS-G18V

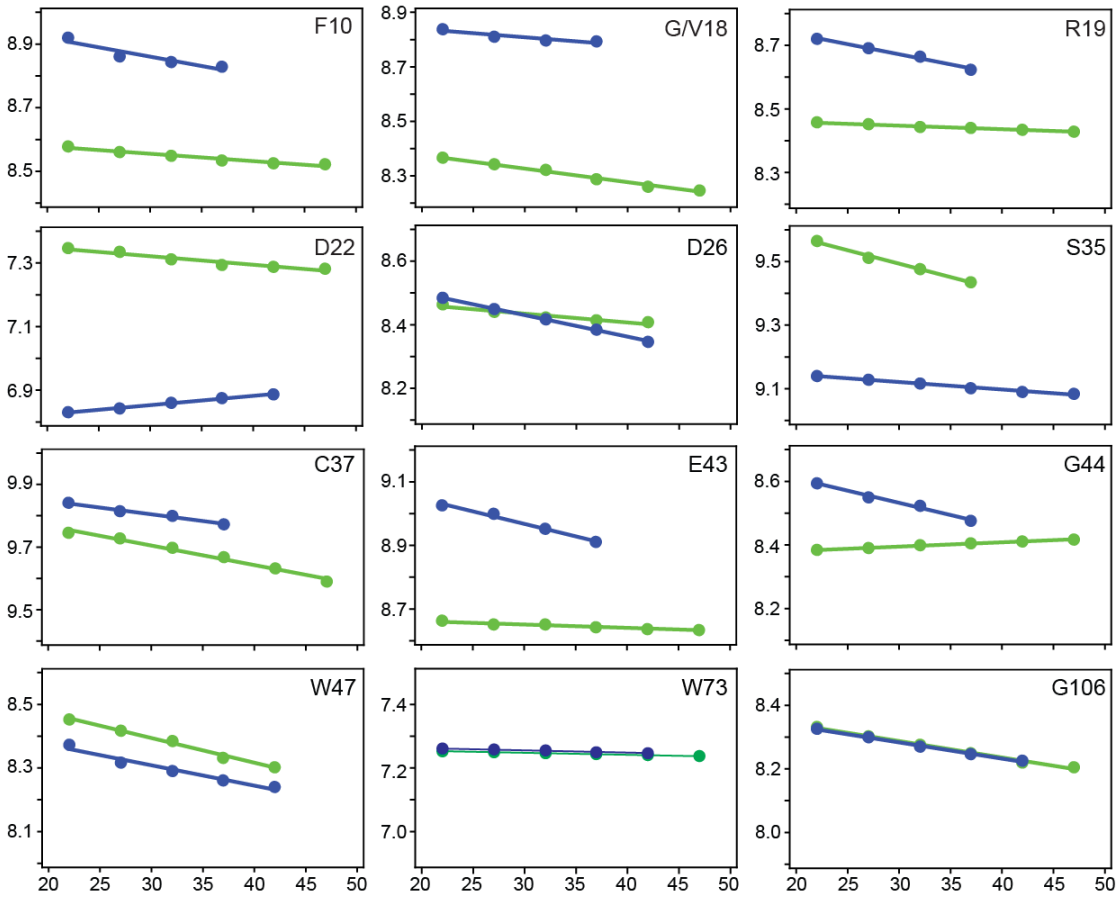

Figure S8: Representative plots comparing the temperature coefficients for the amide protons of residues from γ S-WT and γ S-G18V. Residues where the δ Δ / Δ T value is more positive than -4.6 ppb/K are intermolecularly hydrogen bonded (as in the case of W73 for both proteins), while δ Δ / Δ T values more negative than -4.6 ppb/K indicate hydrogen bonds to solvent (e.g. W47 and G106 for both proteins.)

Table S1: Amide proton temperature coefficients for γS-WT and γS-G18V.

Residue	NH Δδ/ΔT (ppb/K)		Residue	NH Δδ/ΔT (ppb/K)	
	γS-WT	γS-G18V		γS-WT	γS-G18V
S2	-1.22±0.08	-0.58±0.19	I40	-1.03±0.06	-0.96±0.09
K3	-4.80±0.19	-5.25±0.34	K41	-3.46±0.35	-2.50±0.47
T4	2.92±0. 23	-8.46±0.45	V42	-2.44±0.22	-1.84±0.10
G5	-4.00±0.35	-3.30±0.98	E43	1.05±0.12	-7.86±0.68
T6	-5.03±0.28	-4.58±0.37	G44	1.35±0.04	-7.66±0.44
K7	---	-1.50±0.17	G45	1.36±0.15	5.28±0.29
I8	-1.99±0.19	1.00±0.12	T46	-2.26±0.24	-2.92±0.13

T9	-2.15±0.15	-2.62±0.54	W47	-7.76±0.41	-6.40±0.73
F10	-2.31±0.25	-5.88±1.55	A48	-0.40±0.04	-0.86±0.06
Y11	1.33±0.04	1.10±0.17	V49	0.74±0.04	0.68±0.04
E12	-1.21±0.12	-1.54±0.20	Y50	0.87±0.05	1.24±0.10
D13	0.98±0.03	2.36±0.11	E51	-2.86±0.28	-3.16±0.35
K14	0.75±0.21	4.06±0.18	R52	0.87±0.05	0.88±0.02
N15	-2.82±0.12	-2.52±0.40	N54	---	-3.00±0.41
F16	-1.83±0.11	-0.90±0.12	F55	0.84±0.13	3.16±0.32
Q17	1.05±0.16	2.36±0.63	A56	1.05±0.20	1.55±09
G18/V18	-4.98±0.25	-3.00±0.82	G57	-5.25±0.31	-4.82±0.32
R19	-1.12±0.04	-6.36±0.50	Y58	-0.73±0.03	-0.70±0.08
R20	-5.77±0.29	---	I61	-0.45±0.02	-1.09±0.03
Y21	0.61±0.04	-1.30±0.06	L62	-2.33±0.15	-2.84±0.40
D22	-2.69±0.32	2.92±0.12	Q64	-1.69±0.21	-3.90±0.50
C23	1.15±0.19	2.03±0.17	G65	-1.51±0.07	-2.65±0.26
D24	-1.14±0.10	0.26±0.22	E66	-6.09±0.32	-6.65±0.29
C25	----	0.76±0.02	Y67	-1.31±0.08	0.32±0.07
D26	-2.78±0.45	-6.78±0.15	E69	2.10±0.098	1.48±0.12
C27	----	-0.92±0.02	Y70	-3.65±0.46	-4.94±0.24
A28	-1.62±0.33	-1.87±0.30	Q71	-6.93±0.20	-7.80±0.11
D29	1.15±0.07	0.88±0.02	R72	-1.37±0.16	-0.68±0.11
F30	---	-1.15±0.04	W73	-0.63±0.04	-0.70±0.05
H31	1.01±0.04	1.40±0.04	M74	1.74±0.19	1.40±0.06
Y33	0.71±0.03	-0.76±0.11	G75	0.38±0.03	0.58±0.13
L34	4.81±0.14	0.68±0.13	L76	2.73±0.10	0.82±0.12
S35	-8.44±0.51	-2.35±0.11	N77	2.82±0.08	-1.22±0.12
R36	-1.11±0.08	-3.00±0.70	D78	4.21±0.18	3.96±0.22
C37	-6.23±0.37	-4.30±0.21	R79	-3.30±0.07	-3.20±0.07
N38	0.52±0.02	1.16±0.30	L80	0.23±0.02	0.32±0.04
S39	1.08±0.14	1.36±0.14	S81	-0.86±0.38	-1.60±0.19

Residue	NH Δδ/ΔT (ppb/K)		Residue	NH Δδ/ΔT (ppb/K)	
	γS-WT	γS-G18V		γS-WT	γS-G18V
S82	0.89±0.06	1.30±0.06	R125	-1.28±0.05	-1.34±0.10
C83	-1.80±0.03	-1.70±0.06	E126	1.10±0.05	1.07±0.03
R84	-0.31±0.37	-1.00±0.20	I127	-5.18±0.17	-5.00±0.19
A85	-0.34±0.09	5.30±0.36	S129	1.13±006.	0.62±0.03

H87	-2.07±0.26	-6.96±0.97	C130	-2.44±0.14	-1.86±0.32
L88	-8.30±0.34	-1.74±0.19	I138	1.66±0.17	1.44±0.08
S90	---	3.94±0.18	F139	0.75±0.11	0.90±0.08
G91	-1.62±0.06	-3.56±0.10	Y140	0.96±0.03	0.30±0.02
G92	-4.04±0.20	-0.88±0.17	E141	-5.34±0.53	-5.57±0.57
Q93	-2.90±0.09	-3.32±0.08	L142	-0.33±0.02	-0.46±0.04
Y94	-2.53±0.06	-2.78±0.2	N144	0.75±0.08	0.90±0.17
I96	-3.14±0.20	-3.40±0.14	Y145	-1.56±0.10	-1.15±0.06
F99	-2.72±0.30	2.06±0.23	R146	2.19±0.09	2.24±0.08
E100	-4.74±0.34	-4.00±0.13	G147	-4.96±0.30	-4.92±0.17
K101	1.55±0.10	1.43±0.04	R148	-1.38±0.14	-1.18±0.14
G102	-5.84±28	-6.06±0.17	L151	-4.54±0.18	-4.98±0.14
F104	-1.86±0.31	-1.68±0.10	L152	-1.16±0.08	-0.96±0.02
S105	-0.07±0.02	-0.05±0.02	K159	0.58±0.05	-0.45±0.03
G106	-5.17±0.20	-5.10±0.18	I161	-8.30±0.22	-8.42±0.19
Q107	-0.98±0.07	-0.90±0.06	D162	-1.29±0.12	-1.24±0.11
M108	-6.15±0.17	-5.97±0.27	W163	0.68±0.04	0.82±0.05
Y109	-1.02±0.04	-1.06±0.05	G164	-1.15±0.06	-1.51±0.03
E111	-1.50±0.09	-1.88±0.07	A165	-1.84±0.09	-1.90±0.08
T112	-3.88±0.19	-3.90±0.08	S167	1.39±0.08	1.25±0.07
Q113	-0.76±0.10	-0.92±0.16	A169	1.39±0.12	1.39±0.12
D114	-8.54±0.30	-8.46±0.22	V170	3.77±27	2.67±0.23
I115	-1.36±0.14	-1.38±0.17	Q171	-2.87±28	-2.57±0.10
S117	-1.85±0.08	-1.96±0.08	S172	0.33±0.03	0.64±0.047
I118	-1.21±0.09	-1.38±0.13	F173	0.36±0.03	0.68±0.04
M119	-5.13±0.27	-5.30±0.27	R174	1.03±0.06	0.87±0.08
E120	-2.43±0.08	-2.53±0.24	176	2.59±0.12	0.99±0.11
Q121	1.69±0.13	1.53±0.08	V177	-8.25±0.26	-9.20±0.26
F122	-3.23±0.13	-3.24±0.08	E178	-2.10±0.07	-2.10±0.04
H123	0.79±0.03	0.00±0.12			
M124	1.71±0.09	1.65±0.07			

SI References:

(1) Brubaker, W. D.; Freites, J. A.; Golchert, K. J.; Shapiro, R. A.; Morikis, V.; Tobias, D. J.; Martin, R. W. *Biophysical Journal* **2011**, *100* 498.

(2) Franck, J. M.; Pavlova, A.; Scott, J. A.; Han, S. *Progress in Nuclear Magnetic Resonance Spectroscopy* **2013**, *74*, 33.

(3) Armstrong, B. D.; Han, S. *Journal of the American Chemical Society* **2009**, *131*, 4641.

(4) Hausser, K. H.; Stehlik, D. *Advances in Magnetic and Optical Resonance* **1968**, *3*, 79.

(5) Armstrong, B. D.; Han, S. G. *J Am Chem Soc* **2009**, *131*, 4641.

(6) Hwang, L. P.; Freed, J. H. *J Chem Phys* **1975**, *63*, 4017.

(7) Shaka, A. J.; Barker, P. B.; Freeman, R. *Journal of Magnetic Resonance* **1985**, *64*, 547.